ELSEVIER

Applied Surface Science 178 (2001) 7–26

applied surface science

www.elsevier.nl/locate/apsusc

Anisotropic wet chemical etching of crystalline silicon: atomistic Monte-Carlo simulations and experiments

M.A. Gosalvez[a,*], R.M. Nieminen[a,1], P. Kilpinen[b], E. Haimi[b], V. Lindroos[b]

[a]*Laboratory of Physics, Helsinki University of Technology, 02015 Espoo, Finland*
[b]*Laboratory of Physical Metallurgy and Materials Science, Helsinki University of Technology, 02015 Espoo, Finland*

Received 15 November 2000; accepted 2 March 2001

Abstract

An atomic-scale simulation model for anisotropic wet chemical etching of Si(1 0 0)-wafers covered with masks of arbitrary shape and a series of experiments for comparison are presented. The model assumes that the probability of removal of a surface atom depends on the number of first and second neighbors. A removal probability function is presented in order to describe the probabilities of removal corresponding to the different surface atoms having different numbers of first and second neighbors. Etching experiments on Si(1 0 0)-wafers using 10 wt.% KOH solution at 75°C are presented and the performance of the model is evaluated against them. We compare the underetched structures obtained in the simulations and experiments using a mask pattern consisting of a wagon wheel and a set of rectangular frame-like openings with varying orientation. The simulations show good agreement with the experiments. The model predicts the existence of fastest-etched planes in accordance with experiment, and describes accurately the evolution of under-etching below the masks for all mask orientations, including the slopes of the planes appearing below the mask. The results show that the cooperative effects of atoms evolving according to a simple rule generate most features of the meso- and macroscopic etching patterns. They also show that the use of only first neighbors or a partial incorporation of the second neighbors in the modeling strategy is not sufficient in order to describe the under-etching processes and that the second neighbors must be fully incorporated into the model.

Keywords: Anisotropic wet chemical etching; Monte-Carlo simulations; Cellular automaton; Mask; Convex corner; Silicon; KOH; Surface structure; Morphology; Roughness; Topography

1. Introduction

During the last years Micro System Technology (MST) and the manufacture of Micro-Electro-Mechanical Systems (MEMS) have experienced rapid advances. This is partly a consequence of the maturity reached in integrated-circuit technology. However, whilst integrated circuitry focuses essentially on two-dimensional circuit designs, the MEMS community is targeting at three-dimensional micro-structures, such as pressure sensors, resonators, acceleration sensors and gyroscopes. In these devices, both the three dimensional mechanical (and often mobile) parts and the processing electronics are integrated into the same piece of silicon. Not only the reduced device size lowers production costs but also the more precise performance of these micro-devices with respect to

* Corresponding author. Tel.: +358-9-451-3114.
E-mail addresses: mag@fyslab.hut.fi (M.A. Gosalvez), risto.nieminen@hut.fi (R.M. Nieminen).
[1] Co-corresponding author. Tel.: +358-9-451-3105.

0169-4332/01/$ – see front matter
PII: S0169-4332(01)00233-1

their larger counterparts and also the availability of room for innovation makes the field very attractive to both researchers and commercial companies.

Anisotropic wet chemical etching of silicon in alkaline solutions is one of the key techniques for the manufacturing of microsystems. However, a full understanding of the microscopic physics involved has not yet been obtained. The use of atomic scale simulations is proving beneficial towards this aim. In addition, the availability of powerful anisotropic etch simulators would reduce product design costs as well as the times involved.

The paper is organized as follows. In Section 2, we give an overview on some of the alternative methods that may be used to simulate anisotropic wet chemical etching. In Section 3.1, we present a short review of previous works, pointing out their abilities and deficiencies in an attempt to motivate our model, which is presented in Section 3.2. The reason for the choice of the particular functional dependence through a removal probability function and the implications of this choice are discussed in Section 3.3. In Section 4, we give the details of the etching experiments used to validate the model. The simulation and experimental results are presented in Section 5 and comparison and discussion of the performance of the simulation model is done in Section 6. We present our conclusions in Section 7. A detailed account on the implementation aspects of the model is presented in the Appendix A.

2. Background

In situ scanning tunneling microscopy and electrochemical studies [1,2] suggest that the reaction responsible for wet chemical etching of silicon in alkaline solutions actually occurs through both chemical and electrochemical reaction routes. According to these studies the hydroxyl group OH^- plays an important role, catalyzing the removal of surface atoms by favoring further attack at the back bonds. The way how the first hydroxyl group substitutes a terminating hydrogen constitutes the difference between the chemical and electrochemical routes. In the former, a H_2O molecule interacts directly with the terminating H and, as a result, the OH group bonds to the surface atom and a H_2 molecule is formed. This reaction occurs only at kink sites, where enough empty space is available for the process to happen. On the other hand, the electrochemical route involves the dissociation of the Si–H group by direct interaction with an OH^- group, producing a H_2O molecule and a negatively charged state $\equiv Si^-$. In the presence of a H_2O molecule, this state will lead to OH termination if double electron injection to the conduction band is provided. This reaction will occur at any surface configuration (not only at kink sites) but it implies a high activation barrier due to the double electron injection. It provides an isotropic component to the reaction process, although energetically less favorable than the chemical route at kink sites (anisotropic component). Although there is still discussion about the role of OH^- and H_2O in the reaction mechanism, it will be assumed in this work that the OH^- groups catalyze the reaction by weakening the back bonds.

A number of different strategies for the simulation of anisotropic wet chemical etching have been presented in the literature. However, two major approaches can be identified. Within the *geometrical simulators* [3–13] the crystal is reduced to a finite set of crystallographic planes for which the etch rates are known. The surface of the crystal is approximated by a set of these planes, and the time evolution is discretized. Within each time step, each plane forming part of the surface evolves along its normal direction, experiencing a displacement according to the known etch rate for that particular plane. The change in geometry at the intersecting lines between adjacent crystallographic planes or at the edge of a masked region is determined using the Wulff–Jaccodine method [3,4]. In the ideal case, these simulators require the knowledge of complete etch rate diagrams, to be obtained experimentally [5,6]. The more complete the etch rate diagram is, the more accurate the geometrical etch simulator will become. However, only a finite set of etch rates can be accessed experimentally. Nevertheless, several 2D simulators have been reported in the literature [7–9]. Their extension towards 3D problems has proven difficult and performance slow, mainly because new crystal faces can emerge at vertices and edges and the number of possibilities becomes large in 3D. In spite of these difficulties, a number of 3D etch simulators have been reported [10–13].

The second family of anisotropic etch simulators is based on the *atomistic models* [14–18]. In these the

crystal is described at a more microscopic level as a collection of cells or, in some cases, atoms. The neighborhood of an atom or a cell at the surface directly affects the probability with which the etchant can break its backbonds to the rest of the structure and the atom or cell is removed or remains attached accordingly. Due to the randomness involved in the removal of atoms or cells, the evolving crystal surface shows roughness at various scales, a feature which is observed experimentally.

Within the atomistic approach it is possible to make a distinction between Cellular Automaton-based (CA) and Monte-Carlo-based (MC) simulations. These differ in the way how the time evolution of the crystal surface is handled. In the CA approach, at each time step all of the discrete units of the surface (be they atoms or cells) are updated together at once (parallel update). On the other hand, in the MC approach the surface update corresponding to one time step is attained only after N local updates have been tried for a surface containing N atoms or cells (serial update).

Hybrid approaches combining both geometrical and atomistic models have been reported [19,20]. In this work we have targeted at the MC simulation scheme, although both the CA and the MC approaches have been successfully applied on simulating anisotropic etching. We have focused on an atomistic model because it allows a better understanding of the physics involved in the complicated process of dissolution. For instance, it has been shown that these models can offer interesting insights into the study of surface roughness, including local configurations such as triangular pits and pyramidal formations or the propagation of steps along a surface [14–16,21].

3. Description of the model

3.1. Motivation

Previous work by Camon and coworkers [14,15] using Monte-Carlo simulations established a simple stochastic model capable of generating some of the main features observed while etching single crystal silicon (1 0 0) surfaces using masks. They proposed that the probability of removal of an atom at the surface should depend on its neighborhood, which was restricted to the nearest neighbors. For instance, if a Si atom is surrounded by three of its four nearest neighbors in the diamond structure of crystalline silicon, three bonds should be broken in order to remove that atom. This should be a less probable event than the breaking of two bonds in the case of an atom with only two neighbors, which in turn should be less probable than breaking one bond in the case of one neighbor. However, it is easy to notice that the first neighborhood is not enough to establish a difference between certain types of atoms. For instance, both atoms on ideal (1 1 1) and (1 1 0) surfaces have three first neighbors and one dangling bond. In order to introduce a difference between their removal probabilities extra information about the neighborhood has to be incorporated in the model. One way to do this is to take into account not only the number of first neighbors present but also their location with respect to the etch front. This was done by Camon and coworkers [14,15] within a MC scheme and by Than and Büttgenbach [17,18] by using a CA approach. As Than and Büttgenbach noticed [17], this is actually a way of including second-nearest neighbor effects, but only partially and indirectly. In this way, by analyzing the number of nearest neighbors and their location with respect to the etch front for atoms at the three main low index crystallopraghic planes (1 0 0), (1 1 0) and (1 1 1), they derived a set of transition rules to be applied for every atom at any surface, in the hope that the anisotropy would show up itself due to the various combinations of the three previous bonding situations in any particular crystal surface.

This approach, however, although very inspiring, was shown to be insufficient by Camon et al. in a later work [16]. In this case, the probability of breaking a bond between first neighbors was considered. The reason behind was that for surface atoms there is experimental evidence [22] that their dangling bonds are soon populated by hydroxide ions (OH^-) from the etching solution, which ultimately leads to a weakening of the backbond of the corresponding atom. They reasoned that the energy cost of breaking a backbond would depend on the number of hydroxide ions bonded to the atoms sharing the bond in question. By symmetry considerations about the different possible configurations in which hydroxide ions can be bonded to the two silicon atoms sharing the target bond, they found that there would exist eight

different energies, although finally they used four in their simulations. This new approach can be seen as an indirect way to include all effects from the interaction between second-nearest neighbors. In a similar spirit but using different means, it is our purpose to present here an explicit dependence of the probability of removal of an atom as a function of the number of, not only nearest neighbors, but also second-nearest neighbors.

3.2. The model

Some of the considerations and assumptions of our model are based on the work by Camon et al. [16]. However, instead of targeting at the probability of breaking particular bonds, we focus on the description of the probability of removal of an atom as an explicit function of the number of nearest and second-nearest neighbors. The considerations and assumptions of our model are as follows:

- The Si atoms lie at the locations of a diamond structure.
- The neighborhood of an atom contains both nearest and second-nearest neighbors (or, simply, 'first' and 'second' neighbors). The neighborhood comprises in this way a 'first neighborhood' and a 'second neighborhood'.
- An atom is considered to be at the surface if the number of first neighbors is less than or equal to 3. Such atoms are referred to as 'surface atoms'.
- When a surface atom leaves, each first neighbor is left behind with one additional dangling bond, which is quickly paired by a hydroxide ion from the etching solution. For each first neighbor, this results in the weakening of the Si–Si backbonds to the rest of the structure. Therefore, when a surface atom is removed, the energy cost of breaking the bonds to its first neighbors depends not only on the number of first neighbors missing (i.e. hydroxide ions directly linked to the atom) but also on the number of missing second neighbors, because the presence of hydroxide ions in their locations additionally weakens the bonds which still keep the atom linked to the current first neighbors. This dependency on the number of first and second neighbors missing can be stated as a dependency on the number of first and second neighbors that are still present in the neighborhood. One number is related to the other by a simple subtraction from the maximum possible number of first or second neighbors, 4 and 12, respectively.
- The probability of removal of an atom with n_1 first neighbors and n_2 second neighbors, $p(n_1, n_2)$, is described by the following removal probability function:

$$p(n_1, n_2) = p_0 \frac{1}{1 + \mathrm{e}^{\beta\epsilon_1(n_1 - n_1^0)}} \frac{1}{1 + \mathrm{e}^{\beta\epsilon_2(n_2 - n_2^0)}}$$

  where $\beta = 1/k_\mathrm{B}T$, $p_0 = (1 + \mathrm{e}^{-\beta\epsilon_1 n_1^0})(1 + \mathrm{e}^{-\beta\epsilon_2 n_2^0})$ is used to satisfy $p(0,0) = 1$ and $\epsilon_1, \epsilon_2, n_1^0$ and n_2^0 are the parameters of the model. The parameters ϵ_1 and ϵ_2 may be thought as average energies of the interaction between first neighbors and between second neighbors, respectively. We assume that the energy of an atom with n_1 first neighbors and n_2 second neighbors is simply $E(n_1, n_2) = \epsilon_1 n_1 + \epsilon_2 n_2$. If only the first neighborhood is considered, we note that n_1 is a measure of the energy cost of the removal of an atom with n_1 first neighbors in units of ϵ_1. Therefore, ϵ_1 may be understood as the average energy cost of breaking one bond between first neighbors. Similarly, ϵ_2 may be considered as the average energy cost of suppressing the interaction between second neighbors.
- The other two parameters, n_1^0 and n_2^0, can be understood as follows. The parameter n_1^0 is a threshold energy (in units of ϵ_1) below which an atom interacting only with its first neighbors will be dissolved at zero temperature, $T = 0$. Since n_1^0 is measured in units of ϵ_1, it also represents the average number of first-neighbor bonds that are broken at zero temperature as a result of the activity of the etchant. In this way, if the number of first neighbors, n_1, is less than n_1^0 then the atom will most likely be removed by the etchant at a finite temperature. Similarly, n_2^0 is a threshold energy (in units of ϵ_2) below which an atom that interacts only with its second neighbors will be dissolved at zero temperature. At a finite temperature, the atom will most likely be removed by the etchant if the number of second neighbors, n_2, is less than n_2^0.
- The time evolution is realized by using a Monte-Carlo scheme.
- Surface diffusion of an atom before removal and surface reconstruction are not considered.

- Although the model does not take into account the effect of different etching solutions or silicon properties such as the doping level, dependencies through the factor p_0 may be included in the model.

The implementation aspects of the model are presented in the Appendix A.

3.3. General considerations

The particular functional dependence through the removal probability function presented here deserves some comments. While developing the model, we noticed that in order to capture the anisotropy of the etching process it is necessary to introduce large differences between the removal probabilities of atoms with the same first neighborhood and very similar second neighborhoods (which might differ by only one or two second neighbors). For instance, the atom at the edge between planes (1 0 0) and (1 1 1) in Fig. 1 has seven second neighbors in comparison to nine for a typical atom at the (1 1 1) plane, both having identical first neighborhood. The removal probabilities for these atoms should differ by about four orders of magnitude to provide significant under-etching below certain mask corners. Similarly, for atoms located at ideal (1 1 1) and (1 1 0) planes, a difference of the same order is required so that the etch rates of (1 1 1) and (1 1 0) planes differ by about two orders of magnitude, as in experiments [22]. Additional similar cases can be found. These considerations suggest a step-like functional dependence of the probability of removal as a function of the number of second neighbors with the step-like sharp decrease located at about seven or eight second neighbors.

A similar step-like functional dependence can be suggested for the probability of removal as a function of the number of first neighbors. Now the step should be placed at around three first neighbors so that atoms with four first neighbors (bulk atoms) have a negligible probability of removal. For simplicity, the simple product of these two step-like functions is suggested in order to build up a removal probability function to describe the removal probabilities of all possible cases involving any number of first and second neighbors.

As shown in Fig. 2, the most important feature exhibited by the removal probability function is a sharp step-like decrease for those values of n_1 and n_2 which are greater than the threshold values n_1^0 and

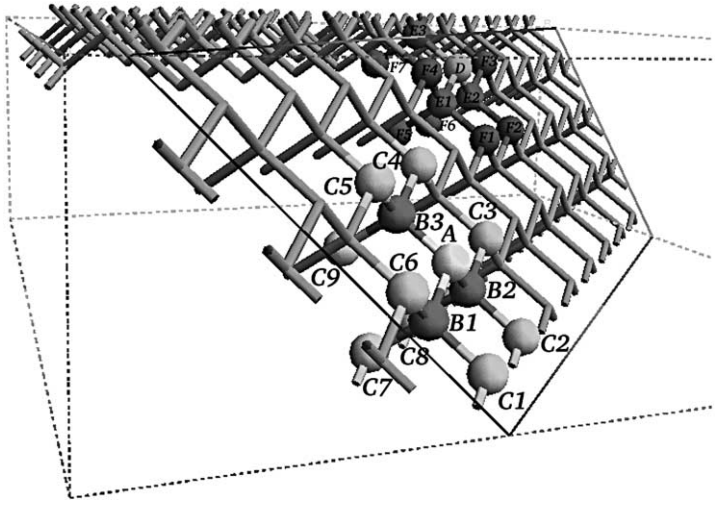

Fig. 1. Two atoms with the same first neighborhood and similar second neighborhood. The figure shows a (1 0 0) plane nearly perpendicular to the plane of the paper and a (1 1 1) plane highlighted by a contour line. The dangling bonds of the atoms of this last plane are not shown for clarity. Closer to the observer, atom A is chosen as an example of a typical (1 1 1) atom having three first neighbors (B1–B3) and nine second neighbors (C1–C9). Further to the back, the neighborhood of atom D at the edge between the two planes is depicted. This atom has also three first neighbors (E1–E3) but only seven second neighbors (F1–F7). The second neighbors corresponding to C4 and C5 are missing.

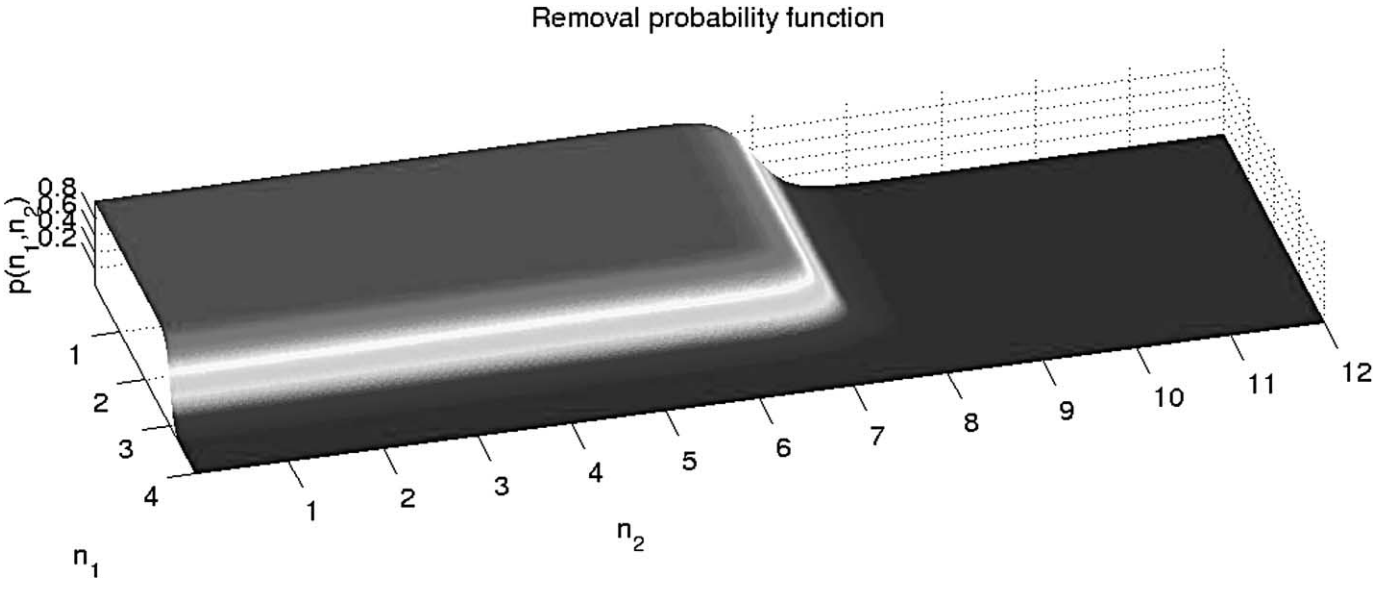

Fig. 2. Removal probability function at $T = 348$ K (75°C) when the model parameters take the values: $\epsilon_1 = 0.35$ eV, $\epsilon_2 = 0.16$ eV, $n_1^0 = 3.0$ and $n_2^0 = 7.0$. This function gives the probability of removal of an atom with n_1 first and n_2 second neighbors.

n_2^0, respectively. Focusing, e.g. on the first neighborhood factor, $1/(1+e^{\beta\epsilon_1(n_1-n_1^0)})$, it is clear that at $T=0$ this is just a step function with the step located at $n_1=n_1^0$. At any other finite temperature the step will exhibit certain width which can be controlled by adjusting the ϵ_1 parameter. Therefore, from a mathematical point of view, n_1^0 controls the position of the step and ϵ_1 its width. By adjusting both ϵ_1 and n_1^0 the relative values of the probabilities of removal of surface atoms linked to one, two or three first neighbors can be controlled in an easy manner. The same arguments can be applied to the second neighborhood factor, $1/(1+e^{\beta\epsilon_2(n_2-n_2^0)})$. By adjusting both ϵ_2 and n_2^0 the relative values of the probabilities of removal for surface atoms with different numbers of second neighbors can be controlled easily.

The functional form presented implies that the removal of an atom is thermally controlled only indirectly through *successive thermal breaking of the chemical backbonds to the rest of the structure*. According to Camon et al. [16], the breaking of the backbonds is a thermally activated process and consequently the probability of breaking, e.g. the bond between atoms i and j, P_{ij}, is related to the activation energy of the process (i.e. the energy of the bond), E_{ij}, through an Arrhenius expression of type $P_{ij}=\lambda\exp(E_{ij}/k_BT)$. In turn, the probability of removal of an atom described by the removal probability function differs from the Arrhenius expression. Consequently, the removal of an atom is only indirectly controlled by temperature.

We notice that the functional form presented here is a convenient mathematical parametrization for the probabilities of removal of surface atoms. It simplifies the amount of effort by the user since it becomes easier to adjust a reduced number of parameters than to adjust the removal probabilities themselves one by one for the large number of possible cases that appear when combining all possible first and second neighborhoods.

4. Experimental

Double side polished $P+(1\,0\,0)$ Czochralski wafers were used in the etching experiments. The wafers were wet oxidized at 1050°C and the thickness of the grown oxide became approximately 1.5 μm. The test mask pattern was lithographically transferred to the oxidized wafers.

The test mask patterns studied included a wagon wheel pattern and a set of rectangular openings with a rectangular oxide island in the middle. These rectangular frame-like openings were located along the outer circle of the wafer, every 3°, with the longer dimension parallel to the radial directions. One of the rectangular patterns was aligned with the ⟨1 1 0⟩ direction of the (1 0 0) wafer surface. This direction is taken as the origin of the angles used to refer to each rectangular frame-like opening. Fig. 3 shows a part of the mask patterns.

The etching experiments were performed in 10 wt.% aqueous KOH solution at 75°C temperature. In the experiments 10 wafers were etched approximately to 70 μm depth. Before etching the wafers were cleaned by RCA1 cleaning process and after etching the wafers were rinsed in DI water. The etching solutions were mixed from high purity, p.a. quality KOH pellets (Merck) and DI water.

Sixteen optical microscope images of the underetched rectangular oxide islands within the range of angles of 0–45° are presented in the upper part of Fig. 3 and in more detail in Fig. 5. The anisotropy of the etching process is revealed by the difference in the amount of lateral underetching occurring at the sides of different rectangular oxide islands and, especially, by the underetching of corners, where fastest-etched planes appear. The difference in lateral underetching at the longitudinal sides of the spokes in the wagon wheel leads to characteristic flower-like patterns such as the one shown in Fig. 4 and thus also provides a method to qualitatively detect anisotropic etching.

The lateral underetch rates for the islands at 0° and 45° correspond to the etch rates of (1 1 1) and (1 0 0) crystal planes, respectively, except for a geometrical factor accounting for the fact that the lateral underetch rate is actually a measure of the projection of the etching rate of the plane in question onto the wafer surface [22]. In the present experimental conditions, the fastest underetch rate was observed for the rectangular oxide island at 27°. This underetch rate is assumed to correspond to the projection of the etch rate of (31X) planes (where X can be 1, 2 or 3) since these planes intersect the (1 0 0) wafer plane at an angle of 26.57°.

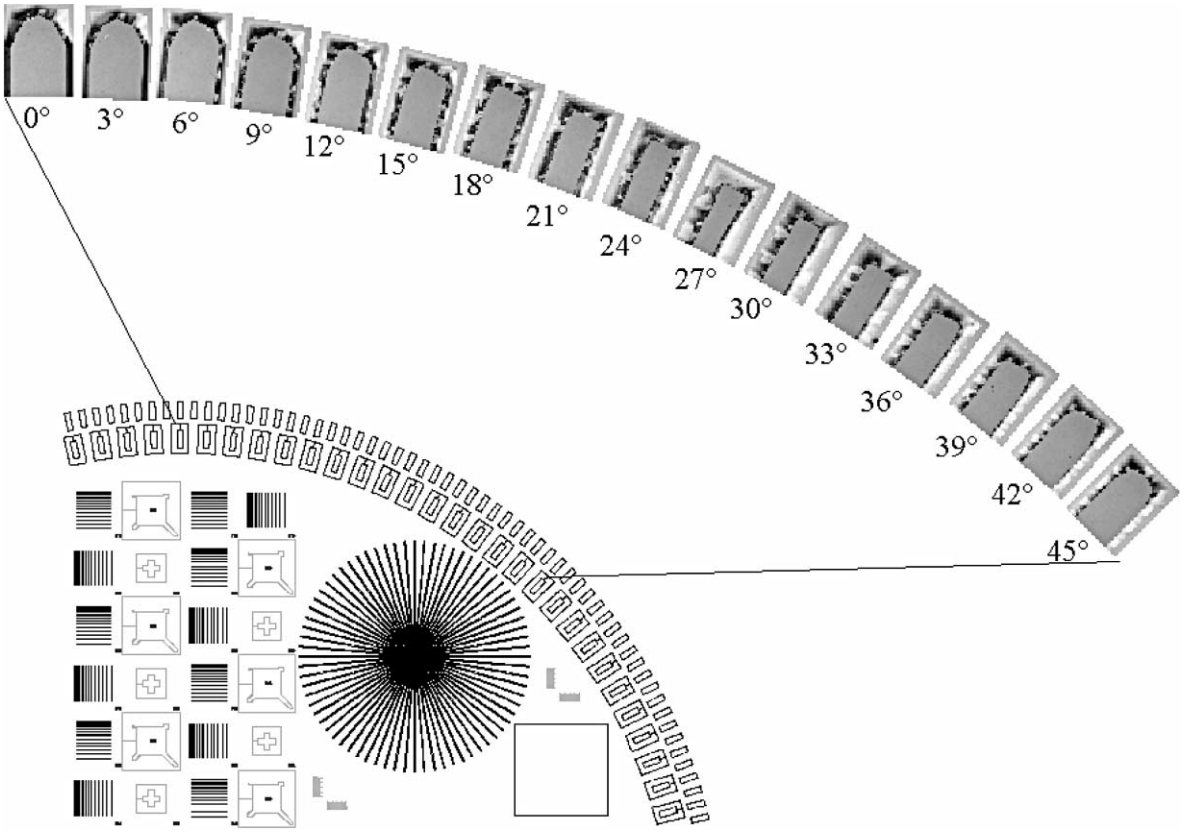

Fig. 3. Part of the test mask pattern showing the rectangular frame-like openings on the outer circle of the wafer repeated every 3°. The blow-up picture shows 16 optical microscope pictures of the underetched rectangular islands within the orientation range of 0–45°. The origin of angles is the ⟨1 1 0⟩ direction contained by the (1 0 0) wafer surface. The results for the blow-up detail were obtained using 10 wt.% KOH solution at 75°C.

5. Simulation results and comparison to experiment

We present in this section the results of the etching simulations for two types of masking structures: half of a wagon wheel and 16 rectangular frame-like openings with varying orientation, as described in the experimental part (Section 4). We will compare them with the results from the etching experiments for the same masking structures obtained using 10 wt.% KOH solution at 75°C. The simulation results presented here were obtained using $T = 348$ K (or 75°C) and the following values of the parameters of the model: $\epsilon_1 = 0.35$ eV, $\epsilon_2 = 0.16$ eV, $n_1^0 = 3.0$ and $n_2^0 = 7.0$.

The results from the etching experiment and the corresponding etching simulation for half of a wagon wheel are shown in Fig. 4. The planar size of the simulated system is 600×600 unit cells or about $0.35\,\mu\text{m} \times 0.35\,\mu\text{m}$ and the corresponding size for the experiment is about $10\,\text{mm} \times 7\,\text{mm}$. Although the difference in size is about five orders of magnitude, good qualitative agreement is observed. 150 Monte-Carlo time steps were required to obtain the results shown in the figure. The size of the final system was $600 \times 600 \times 9$ cells, containing more than 2.6×10^7 atom positions with approximately 9×10^5 atoms at the surface. The typical CPU time required for such simulation is about 7 min using one R12000 processor working at 300 MHz in a SGI Origin 2000 machine

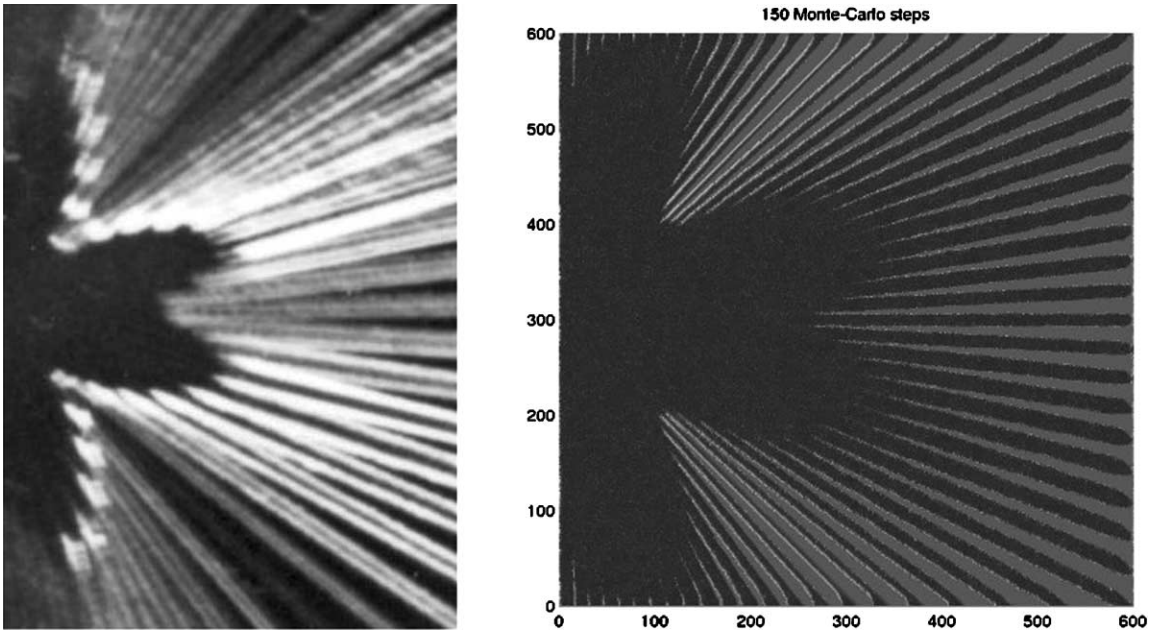

Fig. 4. Comparison between experiment (left) and simulation for a mask consisting of half of a wagon wheel. The angular distance between two spokes is 5° for the experiment and 3° for the simulations. The planar size of the simulated system is 600×600 unit cells (about $0.35\,\mu m \times 0.35\,\mu m$) and the diameter of the full experimental wagon wheel is 20 mm, of which only a region of about $10\,mm \times 7\,mm$ is shown.

and about 4 min using one Alpha 21264 EV67 processor running at 667 MHz.

Fig. 5 shows the experimental results for the 16 rectangular frame-like openings and Fig. 6 presents the corresponding results from the simulations. In this case the planar size of the simulated systems is 400×400 unit cells or about $0.23\,\mu m \times 0.23\,\mu m$ and the corresponding size for the experiments is several hundreds of microns, as shown in Fig. 5. In this case, 500 Monte-Carlo time steps were required to obtain the simulation results shown in Fig. 6. The typical size for the final systems was $400 \times 400 \times 24$ cells, containing more than 3.0×10^7 atom positions with approximately 3×10^5 atoms at the surface. The typical CPU time required for such simulations is about 26 min using the R12000 processor and about 16 min using the Alpha work station.

We present in Figs. 7–10 a graphical comparison of the experimental and simulation results for the rectangular frame-like openings for all the orientations considered. In this case, details corresponding to the results presented in Fig. 6 are shown. The shiny features around the polygonal forms in the experimental frames (left) are due to the wavy shape acquired by the part of the oxide mask which is no longer supported by the silicon crystal. This wavy shape is in turn due to the expansion that this region of the oxide mask experiences relative to the strained region (right on top of the remaining silicon crystal), still under stress due to the silicon-to-oxide unit cell mismatch.

6. Discussion

From the inspection of Figs. 4–6 we conclude that the proposed model reproduces the experimental results to a good accuracy and with significant details. In the case of the wagon wheel in Fig. 4, a flower-like pattern is clearly obtained in both cases. Fig. 4 suggests that the fastest etched plane is well predicted by the model. However, when comparing Figs. 5 and 6and specially after inspection of Fig. 9, it is possible to conclude that the fastest etched plane occurs at an

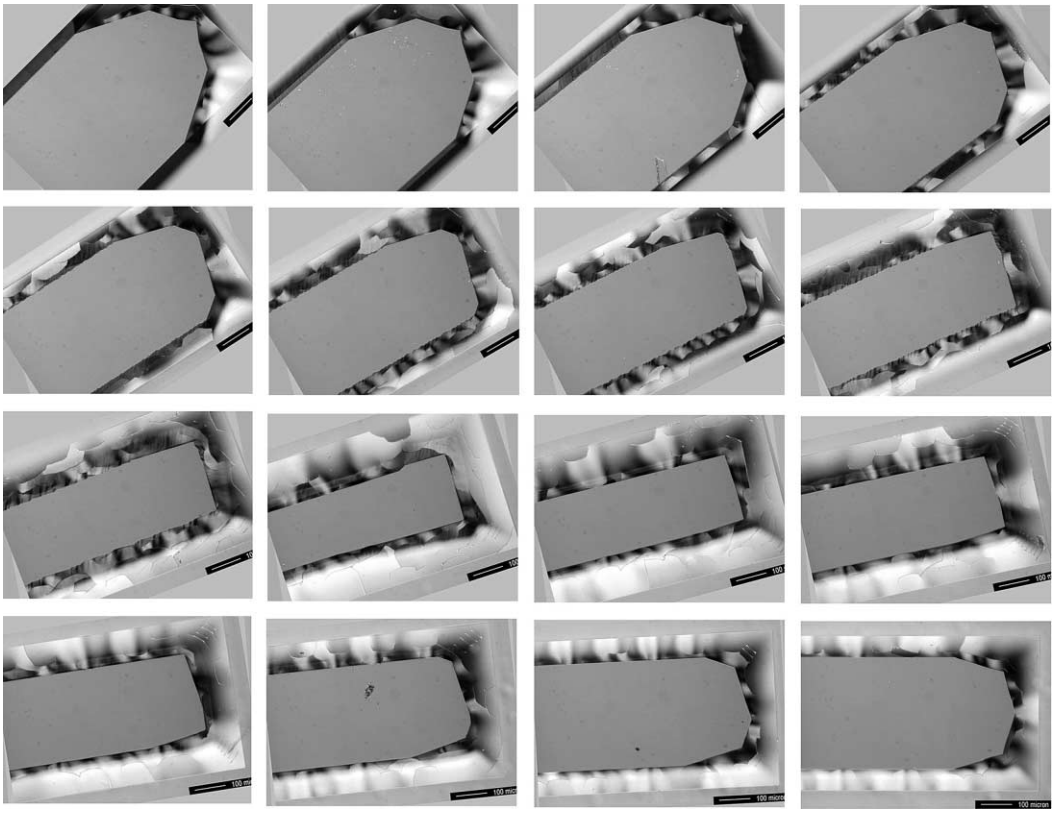

Fig. 5. Experimental results showing underetching below the mask for the oxide islands corresponding to the 16 rectangular frame-like openings. From left to right and from top to bottom, the orientation of the initial rectangular oxide islands ranges from 0° to 45°. The zero angle is defined by the ⟨1 1 0⟩ cristallographic direction, which is aligned with the axis of symmetry of the top-left frame. Underetching of only one end of the rectangular oxide islands is shown. For presentation purposes, the lower-left corner area of all frames (except for the one at the lower-right corner of the figure) shows an artificial line due to the rotation of the experimental pictures shown in Figs. 7–10.

angle between 24° and 30° in the experiment, most probably below 27°, whilst it shows up at a somewhat greater angle in the simulation, between 24° and 33°, most probably closer to 30° than to 27°. Nevertheless, the series of frames from the simulations depicted in Fig. 6 shows the same trend in the evolution of underetching exhibited by the experimental series in Fig. 5.

One feature from the experiment that is well captured by the model is the set of slopes of the etch bordering planes. This is best observed by inspection of Figs. 7–10. For the island oriented at 0° (frames 1.a and 1.b in Fig. 7) underetching does not occur below the longitudinal edges of the masking island. As corresponds to {1 1 1} planes, the slope of the planes that appear in both the experimental and the simulated systems is 54.7°, as measured from the wafer's (1 0 0) plane. The (31X) or (41X) planes ($X = 1$, 2 or 3) that are observed in the experiment below the masking island at the right-end region (corner under-etching) are also obtained in the simulation. In this case, greater roughness is present due to the difference in system scales. The size of the simulated system is not large enough so as to make the rounding effects negligible at the regions where two etch bordering planes intersect and not enough depth has been reached so as to be able to conclude on the nature of those surfaces. Nevertheless, it is remarkable that a good qualitative match is obtained with such a simple model and with such a difference in size scale.

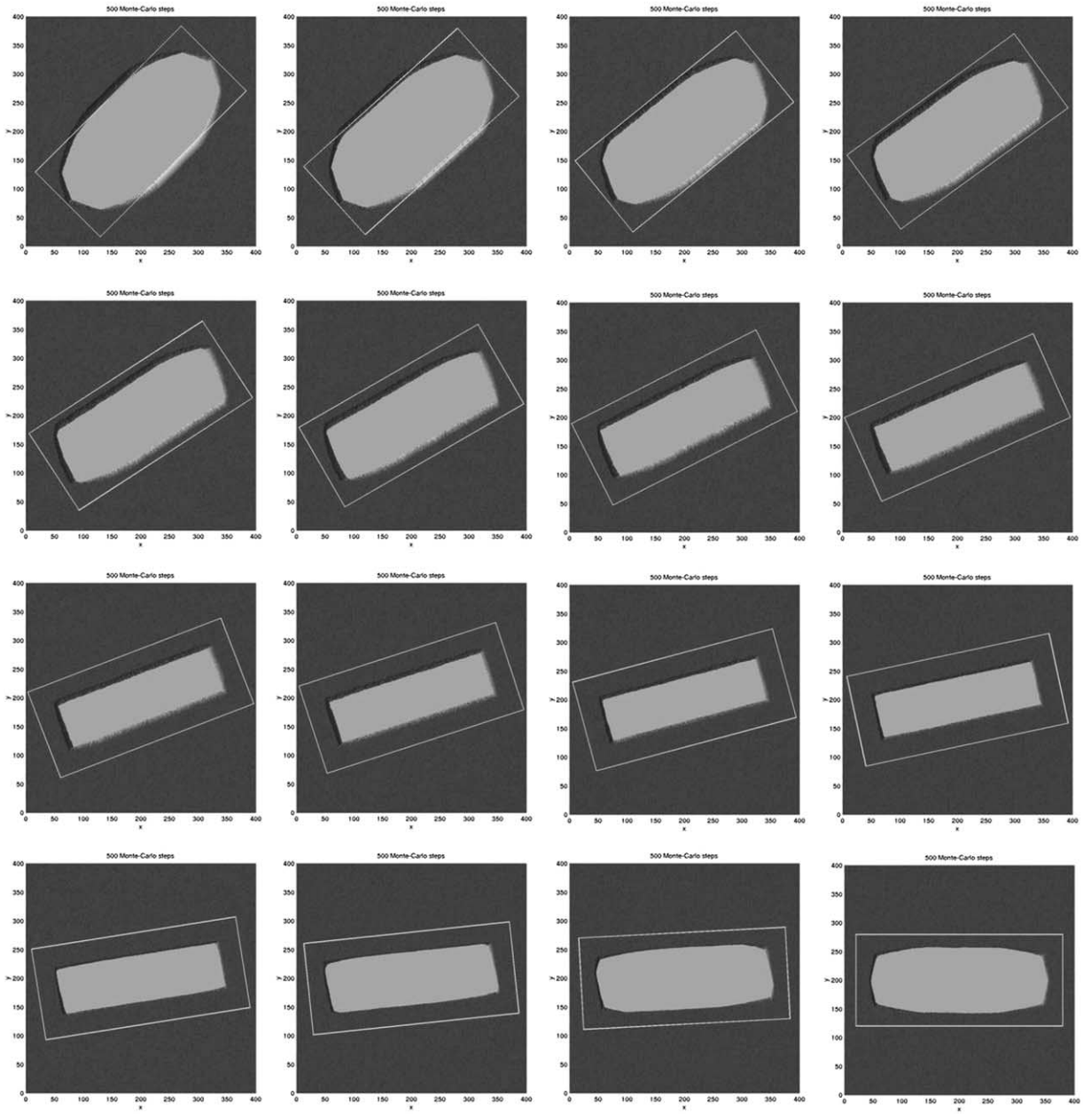

Fig. 6. Simulation results showing underetching below the mask for the oxide islands corresponding to the 16 rectangular frame-like openings. From left to right and from top to bottom, the orientation of the initial rectangular oxide islands ranges from 0° to 45°. The zero angle is defined by the $\langle 1\,1\,0 \rangle$ cristallographic direction, which is aligned with the longitudinal axis of symmetry of the top-left frame. Underetching below the rectangular oxide islands is shown. The thin line describing a rectangular contour in each frame represents the extent of the oxide mask (i.e. the rectangular islands) below which underetching occurs.

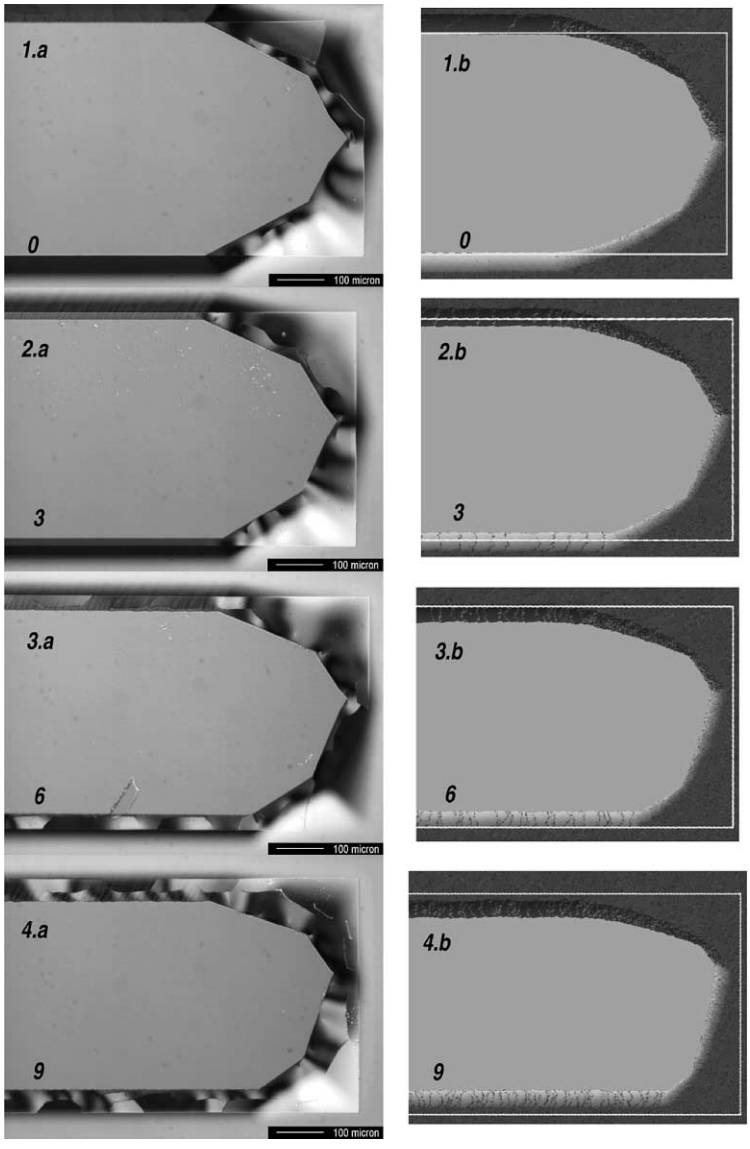

Fig. 7. Comparison of experimental (left) and simulation results. Underetching below one end of the oxide islands is shown for the orientations indicated by the lower-left number (degrees) on each frame. The shiny features around the poligonal forms in the experimental frames (left) are due to the wavy shape acquired by the part of the oxide mask which is no longer supported by the silicon crystal. The thin line describing a rectangular contour in the simulation frames (right) represents the extent of the oxide mask (i.e. the rectangular islands) below which underetching occurs.

Similarly, at the other end of the series (frames 16.a and 16.b in Fig. 10 for 45°), the slopes of the etch bordering planes are once more reproduced. In this case, underetching occurs below the longitudinal edges of the masking island and the slope of the etch bordering planes is nearly 90° in both the experiment and the simulations. As before, the corner underetching at the right-end region made manifest by the appearance of the (31X) or (41X) planes ($X = 1$, 2 or 3) below the masking island is obtained also in the

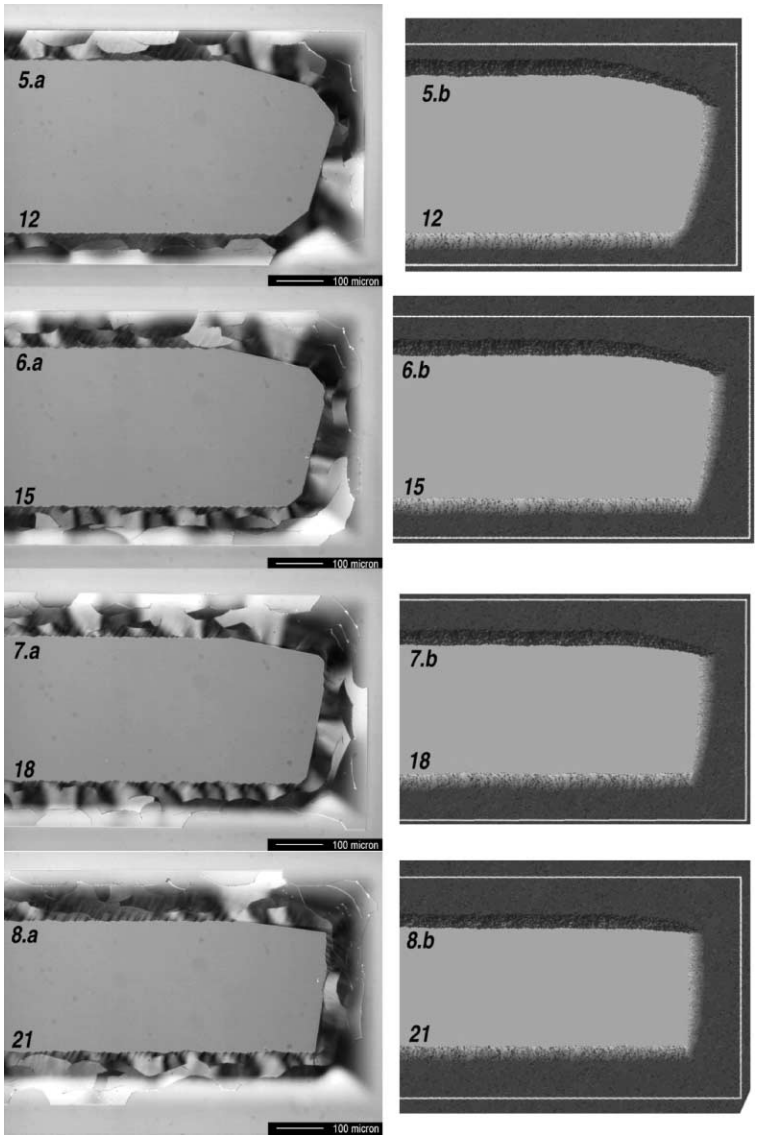

Fig. 8. See Fig. 7.

simulation. From one end of the series to the other, as one goes from frames 2.a and 2.b in Fig. 7 to frames 15.a and 15.b in Fig. 10, a gradual change in these slopes is observed both in the experiment and the simulations.

A major difference between the underetching features of the experiment and the simulations is that, starting from any of the two extreme angles (be it 0° or 45°), the model seems to reach the asymmetric shapes earlier than the experiments. This is best observed when inspecting Figs. 7–10. For instance, in Fig. 7 frame 2.b probably resembles more frame 3.a than frame 2.a and frame 3.b resembles more frame 4.a than 3.a. A similar trend can be discovered for frames at the other end of the series. These differences can be easily understood by the fact that the fastest etched planes are slightly different for the experiment and simulations (at least with the values specified for the

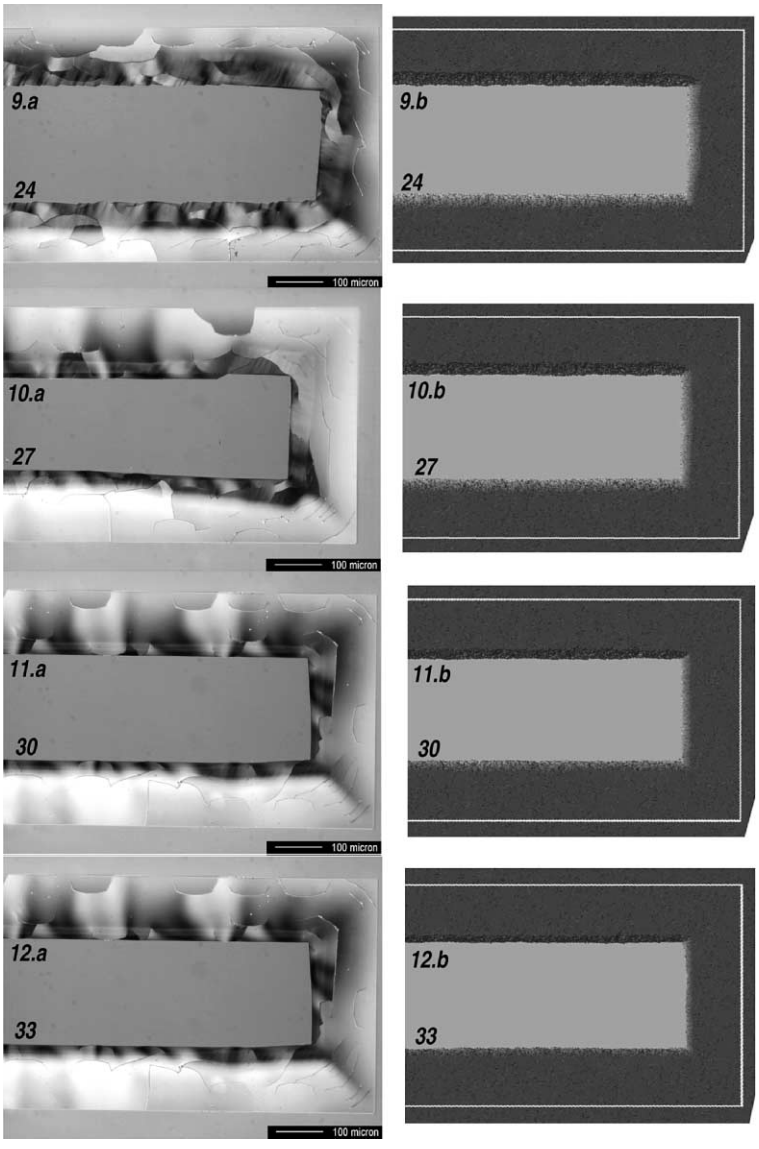

Fig. 9. See Fig. 7.

parameters ϵ_1, ϵ_2, n_1^0 and n_2^0). A slight misorientation of the fastest-etched plane is not so crucial for the two extremes of the series (0° and 45°), because they have an inherent symmetry as the dominant feature (which captures the attention of the viewer), allowing only a secondary role to the misorientation, which in this way is not perceived so clearly. However, the misorientation of the fastest etched plane has clearly an effect on the underetching features for the rest of the series, precisely because of the asymmetry involved in these cases. We believe that a set of values for the parameters of the model can be found which will minimize the small miss-orientation present in our current results.

We point out finally that the model is unable to predict the shape at the very tip of the right-end region of frame 1.a in Fig. 7, at least with the values specified for the parameters ϵ_1, ϵ_2, n_1^0 and n_2^0.

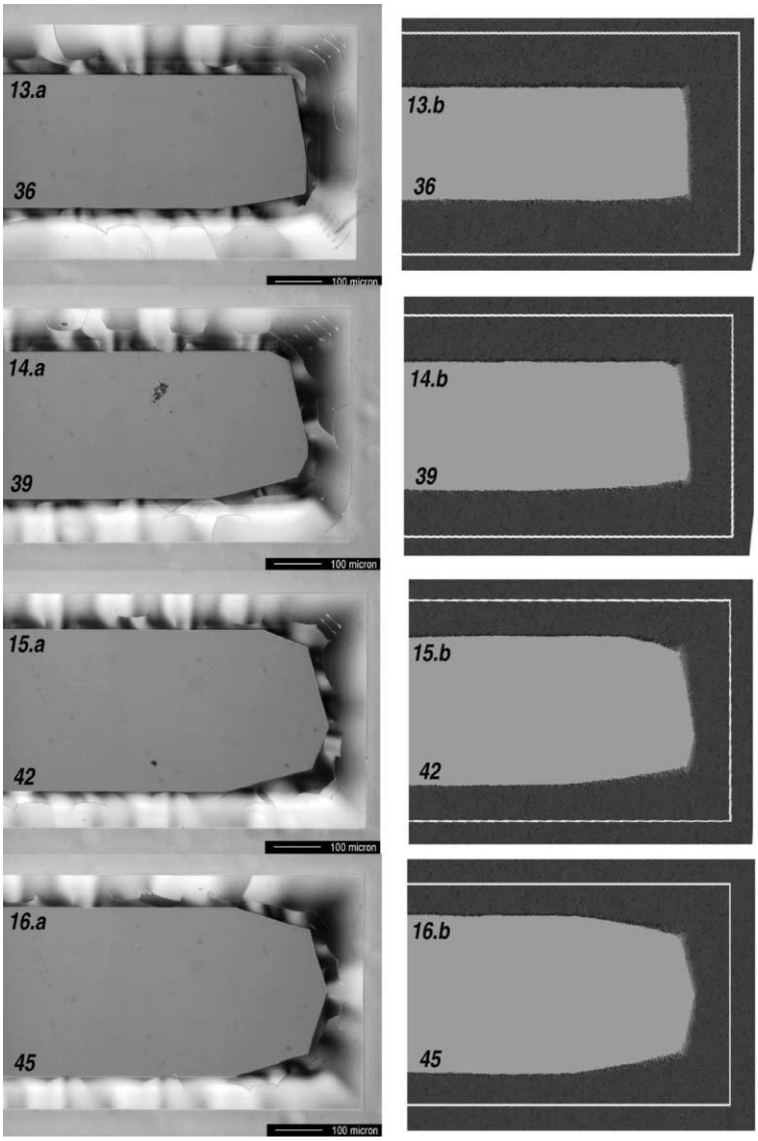

Fig. 10. See Fig. 7.

7. Conclusions

An atomic-scale simulation model for anisotropic etching has been presented and a series of experiments and simulations have been compared in order to validate the model.

The model assumes that the removal of surface atoms by the etchant is a thermally activated process, although only indirectly through activated destruction of the backbonds that keep the atom linked to the rest of the structure. The strength of these backbonds is weakened by quick formation of bonds to hydroxide ions from the solution at the dangling bonds available at surface atoms. In this way the energy cost of the removal of a surface atom depends not only on the number of missing first neighbors (i.e. number of

dangling bonds filled by hydroxide ions), but also on the number of missing second neighbors. Accordingly, the probability of removal of a surface atom is considered to be a function of both numbers of first and second neighbors still present in the neighborhood of the atom.

A removal probability function has been introduced in order to describe the removal probabilities of surface atoms for all possible cases involving any number of first and second neighbors. The physical meaning of the parameters involved in the functional dependency has been discussed and an effort has been made to clarify the reason why the particular functional dependency was chosen.

A series of etching experiments on Si(1 0 0)-wafers using 10 wt.% KOH solution at 75°C has been presented and used to evaluate the performance of the proposed model. We have compared the underetched structures that appear in the simulations and experiments when using mask patterns such as a wagon wheel and a set of rectangular frame-like openings with varying orientation.

The simulations show good agreement with the experiments. The model predicts the existence of fastest-etched planes other than (1 1 0), in accordance with experiment, and describes accurately the evolution of under-etching below the masks for all mask orientations, including the slopes (as measured from the wafer surface) corresponding to the planes that appear below the mask. It is remarkable that such agreement is obtained with a difference in size scales of about five orders of magnitude.

The results show that the second neighbors must be fully incorporated into the modeling strategy in order to describe the under-etching processes to sufficient accuracy. The use of only first neighbors or a partial incorporation of the second neighbors, as has been done previously in the literature, is not sufficient.

Acknowledgements

This research has been supported by the Academy of Finland through its Center of Excellence Program 2000–2001. M.A.G. is thankful to Henry Pinto for his remarks and for his help in the generation of Figs. 1 and 11.

Appendix A. Implementation of the model

The model is implemented as a FORTRAN90 program containing two major computational blocks to handle the initialization of the crystal surface in the presence of any kind of mask (pre-processing) and to implement the Monte-Carlo evolution of the system (processing). A number of output files for further analysis and/or visualization with other tools (post-processing) is generated by the processing block. Before we have a closer look at these procedures we find it necessary to have a brief overview on the most relevant data structures used in the program.

A.1. Data structures

A.1.1. Occupation states

In our model the silicon atoms are located at the lattice sites of the diamond structure, which is built by repeating in the three spatial directions the unit cell basis shown in Fig. 11. The basis contains eight atoms located at the Cartesian positions shown in the left frame of Table 1. A particular atom or lattice site is

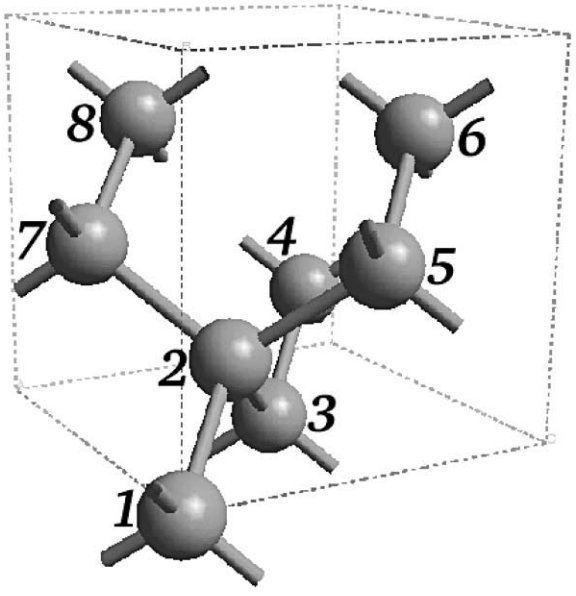

Fig. 11. Unit cell of the diamond structure showing the eight atoms that make up the basis.

Table 1
Unit cell basis; ranges for n_1, n_2, n_3 in a crystal having $N_1 \times N_2 \times N_3$ cells and correspondence between the values of m and l and their meaning are shown

Position	(x_1, x_2, x_3)
1	(0, 0, 0)
2	(0, 0, 0) + (1/4, 1/4, 1/4)
3	(1/2, 1/2, 0)
4	(1/2, 1/2, 0) + (1/4, 1/4, 1/4)
5	(1/2, 0, 1/2)
6	(1/2, 0, 1/2) + (1/4, 1/4, 1/2)
7	(0, 1/2, 1/2)
8	(0, 1/2, 1/2) + (1/4, 1/4, 1/4)
n_1	$1, \ldots, N_1$
n_2	$1, \ldots, N_2$
n_3	$1, \ldots, N_3$
m	(x_1, x_2, x_3)
1	(0, 0, 0)
2	(1/2, 1/2, 0)
3	(1/2, 0, 1/2)
4	(0, 1/2, 1/2)
l	(x_1, x_2, x_3)
1	(0, 0, 0)
2	(1/4, 1/4, 1/4)

referred to by using five integer coordinates (n_1, n_2, n_3, m, l) or '*nml*-coordinates'. The ranges of these coordinates and their corresponding meaning are given in the right frame of Table 1. Two arrays are used to store the 'occupation states' of all lattice sites in the crystal, characterizing simultaneously the existence or not of an atom at every site and the number of first and second neighbors that the atom has currently. The first array, oc1, stores the number of first neighbors and the possible 'occupation states' are: ($nml = (n_1, n_2, n_3, m, l)$).

- $\mathrm{oc1}(nml) = 0$ if site *nml* is not occupied by a Si atom.
- $\mathrm{oc1}(nml) = 1, \ldots, 4$ if site *nml* is occupied by a Si atom with 1, ... , 4 first neighbors.
- $\mathrm{oc1}(nml) = 5$ if site *nml* is occupied by a passivation (oxide) layer atom.

Similarly, the number of second neighbors is stored in the second array, oc2, whose 'occupation states' are

- $\mathrm{oc2}(nml) = h$ with $h = 0, \ldots, 12$ means that site *nml* has h second neighbors.

A.1.2. Use of a dynamic active band and a surface atom list

Only the planar size $N_1 \times N_2$ of the initial system needs to be specified for the simulations. The program dynamically optimizes the third dimension by adding new silicon layers at the bottom of the crystal or eliminating old layers at the top as required by the evolution. This is particularly beneficial when no masks are used, as in the case of studying, e.g. the set-up and evolution of roughness as a function of the values taken by the model parameters. In this case the whole surface evolves by just propagating downwards with some statistical width as silicon atoms are removed and it is only necessary to keep a small number of layers (the 'active band') to represent the crystal structure.

When masks are used, some benefit is also obtained because the initial MC time steps are computationally more efficient due to the smaller third dimension of the system. As time evolves, the third dimension increases and so does the size of arrays oc1 and oc2. This leads to larger use of memory as the simulation proceeds and also to significant slowing down in performance if care is not taken. This is so because ultimately most CPU time will be spent trying to choose randomly surface atoms from the whole crystal (i.e. from oc1), which is growing larger. The use of an extra array storing just the current surface atoms would help. We use an array (surface atom list) which keeps not only the atoms at the current surface but also further space for new atoms becoming part of the surface. Old surface atoms are marked specially when they leave the surface and they are all cleaned at once when no more space is left in the array. After this cleaning, the array is provided once more with additional free space where new surface atoms can be kept. This approach is computationally more efficient than updating the array every time that an atom is removed from or added to the surface because this process occurs very often.

A.1.3. Boundary conditions

We use periodic boundary conditions along the two planar directions, n_1 and n_2. These are easy to implement since all that is required is to cycle the values of

the (n_1, n_2) coordinates when any of them goes out of its range by passing over any of its two extremal values:

$$\left|\begin{array}{l}\text{if } n_i = 0 \Rightarrow n_i = N_i \\ \text{if } n_i = N_i + 1 \Rightarrow n_i = 1\end{array}\right| \quad (i = 1, 2)$$

Within the program, the boundary conditions are used only when looking up the neighbors of an atom.

A.2. Pre-processing: initialization

In a typical simulation in the presence of a mask a file containing information about the mask is used to initialize arrays oc1 and oc2. This is necessary because the number of first and second neighbors for the atoms below the masking layer is different from those for the atoms in contact with the etchant.

The initialization procedure is reduced to an inclusion problem in which the atoms at the top layer of the crystal are checked against being included or not within the 2D polygonal region describing the mask. Since this 2D polygonal region may be non-convex in general, the problem is reduced to an inclusion problem for only convex regions. This is done by describing the initial non-convex 2D polygon as the subtraction of smaller convex regions from a larger also convex region. The problem of checking if an atom belongs to the initial 2D polygon is re-formulated as the problem of checking if the atom belongs to the larger region but is not contained in any of the smaller ones.

In order to know if a given point belongs to the inside of a region we use the sign of the cross-product of each directed segment along the perimeter of the region and the vector joining the start of the segment with the given point. Since we use the notion of directed segments and sequentially cover all the points over the perimeter of the region, the order in which the points of each region are accessed is important. For us the order is always counter-clock-wise. Based on this order, if all the cross-product signs are positive, the point belongs to the region and, if at least one of the signs is negative, then the point is outside. If only one cross product is zero, we assume in a rather arbitrary way that the point is outside the region.

Initialization in the presence of masks is made in three steps:

1. A 'basic initialization' in which all the sites are marked as bulk (i.e. $\mathrm{oc1}(nml) = 4$ for all *nml*-coordinates) except the top crystal layer which is marked as passivation (i.e. $\mathrm{oc1}(nml) = 5$ for the *nml*-coordinates of the sites in the top layer).
2. An 'inclusion initialization' in which all the sites of the top layer which are exposed to the etchant are marked as empty (i.e. $\mathrm{oc1}(nml) = 0$). This step is realized using the inclusion problem ideas presented before.
3. A 'neighborhood initialization' in which, for every atom belonging to the top layer or to the layer just below this one, the first and second neighbors present in the structure are counted and their values are written into oc1 and oc2, respectively.

Initialization without masks can be done using a similar procedure in which the passivation layer does not exist.

A.3. Processing: MC scheme

Fig. 12 shows the flow diagram corresponding to the main purpose of the program. We comment here the different stages with some more detail:

- The program reads in the model parameters, the planar size of the crystal, the mask file name and the number of MC steps to terminate.
- Arrays oc1 and oc2 are initialized using the information from the mask file and the methodology presented in Section A.2.
- The removal probabilities for any type of surface atom are calculated using the removal probability function and stored into an array (probs).
- The simulation is carried out by discretizing the time evolution in MC time steps until the final time $t = T$ is reached. For each MC time step a loop of local-update trial (LUTs) is carried out (counter n). The total number of LUTs inside a MC time step, N, is the number of atoms located at the surface at the beginning of the MC time step. Each LUT occurs at a randomly chosen atom from the current surface. The form of one LUT is as follows:
  - Choose the *nml*-coordinates of one atom from the surface and read off from arrays oc1 and oc2 the number of first and second neighbors, n_1 and n_2.

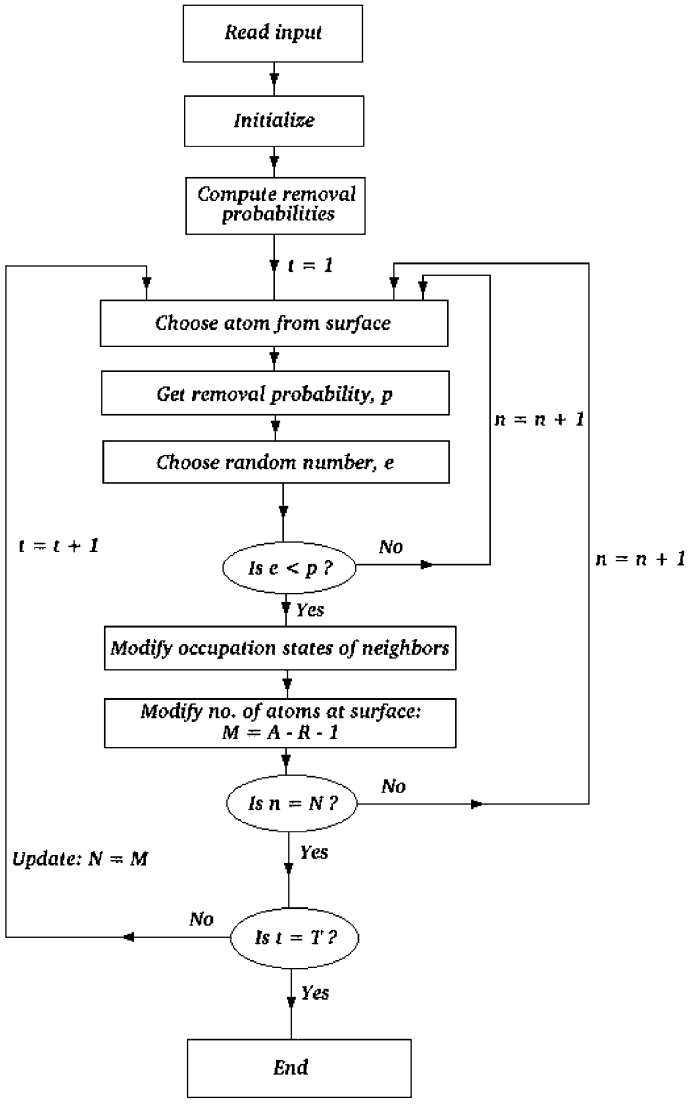

Fig. 12. Flow diagram of simulation program.

- Read off the removal probability (p) for the chosen atom from array probs and n_1 and n_2.
- Choose one random number e between 0 and 1.
- If $e \leq p$ then the chosen atom will be removed but otherwise a new local update will be started again.
  - If the chosen atom is removed, the occupation states of both the first and the second neighbors have to be modified. All that needs to be done is to reduce their occupation states by one unit because the first neighbors will now count one first neighbor less in their neighborhoods and the second neighbors, one second neighbor less.
  - As a consequence of the previous step, the number of atoms at the surface (surface size) needs to be modified. Since the chosen atom was removed, the surface size is reduced by one unit. In addition, a first neighbor might also be removed from the surface if it happened to be linked only to the atom that just left. On the other hand, another first neighbor might

become now a member of the surface if it happened to be in the bulk before the removal of the atom. Therefore, the new surface size is $M = A - R - 1$ where A is the number of first neighbors added to the surface (i.e. first neighbors whose occupation state was four before the removal of the chosen atom) and R is the number of first neighbors that are removed (i.e. first neighbors whose occupation state was 1 before the removal of the chosen atom).

  - If the number of local-update trials n is already equal to the size of the surface at the beginning of the MC time step (N), then a new MC step is initiated with the new size being M. Otherwise, a new local update is tried.

- If the number of MC time steps is already equal to T the program finishes.

A.4. Post-processing

At any desired time, a file containing the Cartesian positions of the atoms at the current surface is created for further analysis. For visualization purposes, a triangulation of the set of points making up the surface is generated. This is actually obtained by projecting the set of points onto the xy-plane after which finding a 2D triangulation is easier than the problem of finding the triangulation of a 2D surface living in a 3D space. A faceted surface in 3D space is drawn using the Cartesian positions of the surface atoms and the triangulation information in order to create the facets. The figures corresponding to the simulations presented in this work were obtained in this way.

References

[1] P. Allongue, Phys. Rev. Lett. 77 (1996) 1986–1989.
[2] P. Allongue, V. Costa-Kieling, H. Gerischer, J. Electrochem. Soc. 140 (1993) 1018–1026.
[3] R.J. Jaccodine, J. Appl. Phys. 33 (1962) 2643–2647.
[4] D.W. Shaw, J. Cryst. Growth 47 (1979) 509–517.
[5] K. Sato, M. Shikida, Y. Matsushima, T. Yamashiro, K. Asaumi, Y. Iriye, M. Yamamoto, Sens. Actuators A 64 (1998) 87–93.
[6] K. Sato, M. Shikida, T. Yamashiro, K. Asaumi, Y. Iriye, M. Yamamoto, Sens. Actuators A 73 (1999) 131–137.
[7] A. Koide, K. Sato, S. Tanaka, in: Proceedings of the IEEE Micro Electro Mechanical Systems Workshop, Nara, February 1991, pp. 216–220.
[8] J. Frühauf, K. Trautman, J. Wittig, D. Zielke, J. Micromech. Microeng. 3 (1993) 113–115.
[9] K. Sato, in: Proceedings of the IEEE 7th International Symposium on Micromachine and Human Science, Nagoya, October 1996, pp. 43–50.
[10] C.H. Sequin, Sens. Actuators A 34 (1992) 225–241.
[11] G. Li, T. Hubbard, E.K. Antonsson, in: Tech. Proceedings of the 1998 International Conference on Modeling and Simulation of Microsystems (MSM 98), Santa Clara, California, USA, 6–8 April 1998, pp. 356–361.
[12] A. Koide, S. Tanaka, in: Proceedings of the IEEE Micro Electro Mechanical Systems (MEMS'97), Nagoya, 26–30 January 1997, pp. 418–423.
[13] K. Asaumi, Y. Iriye, K. Sato, in: Proceedings of the IEEE Micro Electro Mechanical Systems (MEMS'97), Nagoya, 26–30 January 1997, pp. 412–417.
[14] H. Camon, A.M. Gue, J.S. Daniel, M. Djafari-Rouhani, Sens. Actuators A 33 (1992) 103–105.
[15] H. Camon, Z. Moktadir, Sens. Actuators A 46–47 (1995) 27–29.
[16] H. Camon, Z. Moktadir, M. Djafari-Rouhani, Mater. Sci. Eng. B 37 (1996) 142–145.
[17] O. Than, S. Büttgenbach, Sens. Actuators A 45 (1994) 85–89.
[18] S. Büttgenbach, O. Than, in: Proceedings of the IEEE European Design and Test Conference (ED&TC96), Paris, 11–14 March 1996, pp. 454–458.
[19] M. Chahoud, H.-H. Wehmann, A. Schlachetzki, Sens. Actuators A 63 (1997) 141–146.
[20] T.J. Hubbard, E.K. Antonsson, in: Proceedings of the 1996 ASME Design Engineering Technical Conference and Computers in Engineering Conference, Irvine, California, 18–22 August, 96-DETC/DFM-1312.
[21] J. Kasparian, M. Elwenspoek, P. Allongue, Surf. Sci. 388 (1997) 50–62.
[22] H. Seidel, L. Csepregi, A. Heuberger, H. Baumgartel, J. Electrochem. Soc. 137 (1990) 3612–3626.